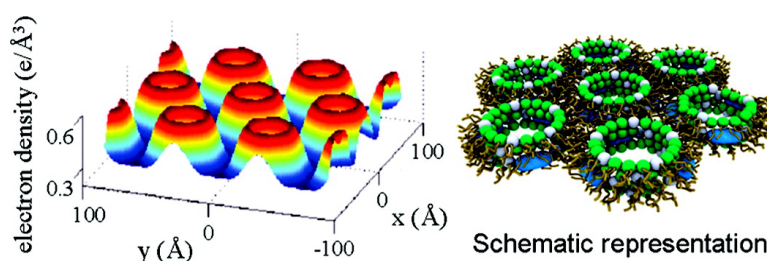**Article**

Synthetic Antimicrobial Oligomers Induce a Composition-Dependent Topological Transition in Membranes

Lihua Yang, Vernita D. Gordon, Abhijit Mishra, Abhigyan Som, Kirstin R. Purdy, Matthew A. Davis, Gregory N. Tew, and Gerard C. L. Wong

Schematic representation

More About This Article

Additional resources and features associated with this article are available within the HTML version:

- Supporting Information
- Links to the 12 articles that cite this article, as of the time of this article download
- Access to high resolution figures
- Links to articles and content related to this article
- Copyright permission to reproduce figures and/or text from this article

View the Full Text HTML

Synthetic Antimicrobial Oligomers Induce a Composition-Dependent Topological Transition in Membranes

Lihua Yang,[†] Vernita D. Gordon,[†] Abhijit Mishra,[†] Abhigyan Som,[‡] Kirstin R. Purdy,[†] Matthew A. Davis,[†] Gregory N. Tew,*,[‡] and Gerard C. L. Wong*,[†]

Contribution from the Departments of Materials Science & Engineering, Physics, and Bioengineering, University of Illinois at Urbana—Champaign, Illinois 61801, and Department of Polymer Science & Engineering, University of Massachusetts, Amherst, Massachusetts 01003

Received April 2, 2007; E-mail: tew@mail.pse.umass.edu; gclwong@uiuc.edu

Abstract: Antimicrobial peptides (AMPs) are cationic amphiphiles that comprise a key component of innate immunity. Synthetic analogues of AMPs, such as the family of phenylene ethynylene antimicrobial oligomers (AMOs), recently demonstrated broad-spectrum antimicrobial activity, but the underlying molecular mechanism is unknown. Homologues in this family can be inactive, specifically active against bacteria, or nonspecifically active against bacteria and eukaryotic cells. Using synchrotron small-angle X-ray scattering (SAXS), we show that observed antibacterial activity correlates with an AMO-induced topological transition of small unilamellar vesicles into an inverted hexagonal phase, in which hexagonal arrays of 3.4-nm water channels defined by lipid tubes are formed. Polarized and fluorescence microscopy show that AMO-treated giant unilamellar vesicles remain intact, instead of reconstructing into a bulk 3D phase, but are selectively permeable to encapsulated macromolecules that are smaller than 3.4 nm. Moreover, AMOs with different activity profiles require different minimum threshold concentrations of phosphoethanolamine (PE) lipids to reconstruct the membrane. Using ternary membrane vesicles composed of DOPG:DOPE:DOPC with a charge density fixed at typical bacterial values, we find that the inactive AMO cannot generate the inverted hexagonal phase even when DOPE completely replaces DOPC. The specifically active AMO requires a threshold ratio of DOPE:DOPC = 4:1, and the nonspecifically active AMO requires a drastically lower threshold ratio of DOPE:DOPC = 1.5:1. Since most gram-negative bacterial membranes have more PE lipids than do eukaryotic membranes, our results imply that there is a relationship between negative-curvature lipids such as PE and antimicrobial hydrophobicity that contributes to selective antimicrobial activity.

1. Introduction

The development of bacterial resistance to conventional antibiotics is a major public health concern. For example, methicillin-resistant *Staphylococcus aureus* (MRSA) and vancomycin-resistant *enterococci* (VRE) and *Staphylococcus aureus* (VRSA) have emerged as common nosocomial (hospital-originating) infections.[1–3] Circumvention of such resistance may be possible by emulating host defense antimicrobial peptides (AMPs), which are found in a broad range of species and have broad-spectrum antimicrobial properties. These AMPs have two structural motifs in common: they are cationic and amphipathic.[4–6] It is thought that electrostatic interactions facilitate association of the peptide with the anionic bacterial membrane[7,8] and amphiphilic interactions act to form pores in the bacterial membrane, leading to cell death. Thus, AMPs target generic characteristics common to the membranes of many pathogenic species, and resistance to such natural defenses evolves much more slowly than for conventional antibiotics.[7] The exact molecular mechanisms by which membrane pores are formed are still not fully understood, although three major models ("barrel-stave", "toroidal pore", and "carpet") have been proposed.[9–16] Moreover, these models do not exhaustively cover all possibilities, as AMP activity is not always correlated with the loss of a permeability barrier. Understanding the structural tendencies generated in antimicrobial—membrane interactions is an essential step toward elucidating such molecular mechanisms and therefore toward the predictive design of synthetic AMP analogues.

[†] University of Illinois at Urbana—Champaign.
[‡] University of Massachusetts.

(1) Tomasz, A. *N. Engl. J. Med.* **1994**, *330*, 1247−1251.
(2) Murray, B. E. *N. Engl. J. Med.* **2000**, *342*, 710−721.
(3) de Sousa, M. A.; de Lencastre, H. *J. Clin. Microbiol.* **2003**, *41*, 3806−3815.
(4) Brogden, K. A. *Nat. Rev. Microbiol.* **2005**, *3*, 238−250.
(5) Boman, H. G. *Immunol. Rev.* **2000**, *173*, 5−16.
(6) Hancock, R. E. W.; Lehrer, R. *Trends Biotechnol.* **1998**, *16*, 82−88.
(7) Zasloff, M. *Nature* **2002**, *415*, 389−395.
(8) Yeaman, M. R.; Yount, N. Y. *Pharmacol. Rev.* **2003**, *55*, 27−55.

(9) Rapaport, D.; Shai, Y. *J. Biol. Chem.* **1991**, *266*, 23769−23775.
(10) Rapaport, D.; Shai, Y. *J. Biol. Chem.* **1992**, *267*, 6502−6509.
(11) Ludtke, S. J.; He, K.; Heller, W. T.; Harroun, T. A.; Yang, L.; Huang, H. W. *Biochemistry* **1996**, *35*, 13723−13728.
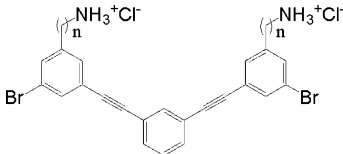(12) Matsuzaki, K.; Sugishita, K.; Ishibe, N.; Ueha, M.; Nakata, S.; Miyajima, K.; Epand, R. M. *Biochemistry* **1998**, *37*, 11856−11863.
(13) Yang, L.; Weiss, T. M.; Lehrer, R. I.; Huang, H. W. *Biophys. J.* **2000**, *79*, 2002−2009.
(14) Zemel, A.; Fattal, D. R.; Ben-Shaul, A. *Biophys. J.* **2003**, *84*, 2242−2255.
(15) Pouny, Y.; Rapaport, D.; Mor, A.; Nicolas, P.; Shai, Y. *Biochemistry* **1992**, *31*, 12416−12423.
(16) Wu, M.; Maier, E.; Benz, R.; Hancock, R. E. W. *Biochemistry* **1999**, *38*, 7235−7242.

Table 1. Structure, Antibacterial Activity, and Hemolytic Activity of AMO-1, AMO-2, and AMO-3

		MIC (μg/mL)			(HC$_{50}$/MIC)	
n	AMO	*E. coli*	*B. subtilis*	HC$_{50}$ (μg/mL)	*E. coli*	*B. subtilis*
1	**1**	>100	>100	>100	N/A	N/A
2	**2**	0.8	1.7	75	93	44
3	**3**	1.6	3.2	3.2	2	1

Over the past decade, new peptidic and nonpeptidic antimicrobial oligomers (AMOs) with tunable structural features similar to those of natural, membrane-spanning AMPs have been synthesized and investigated.[17-33] Like AMPs, these oligomers are also cationic and amphiphilic. However, these synthetic analogues have significantly lower molecular weights and often do not span the membrane. Synthetic AMOs have the advantage that their structures can be tuned so that the importance of electrostatic and amphiphilic interactions to membrane remodeling and cytotoxicity can be systematically probed.

In this paper, we use synchrotron small-angle X-ray scattering (SAXS) to examine the structures made by self-assembly of model membrane vesicles and members of a prototypical class of synthetic AMOs. We chose the *meta*-phenylene ethynylene (mPE) family (Table 1) since its members are simple divalent oligomeric amphiphiles with good antimicrobial activity and selectivity.[32,34] As the hydrophobic volume of these AMOs increases, the homologues in this family can be inactive (AMO-1), specifically active against bacteria (AMO-2), or nonspecifically active against bacteria and eukaryotic cells (AMO-3). We find that the antibacterial activity of these AMOs correlates with their ability to induce an inverted hexagonal (H$_{II}$) phase when added to concentrated small unilamellar vesicle (SUV) suspensions. This phase consists of columnar arrays of lipid tubes

threaded by water channels with diameters of 3.4 nm. When AMO-2 is applied to dilute giant unilamellar vesicle (GUV) suspensions, encapsulated polymers with a diameter less than 3.4 nm leak out, whereas larger polymers are retained. These results suggest a common structural tendency in membrane−AMO interactions, which is expressed as an inverted hexagonal phase in bulk membrane systems and as permeated quasi-2D membranes in isolated vesicles.

The generation of an H$_{II}$ phase requires negative curvature. This provides a potential mechanism for selective activity: most gram-negative bacterial membranes are rich in PE lipids, which have a negative intrinsic curvature, while eukaryotic cell membranes are rich in PC lipids, which have zero intrinsic curvature. Using concentrated SUV suspensions composed of DOPG:DOPE:DOPC (see Note at the end of this paragraph), we find that the inactive AMO-1 cannot generate the inverted hexagonal phase even when DOPE completely replaces DOPC, whereas the specifically active AMO-2 requires a threshold ratio of DOPE:DOPC = 4:1. In contrast, the nonspecifically active AMO-3, which lyses eukaryotic cells, requires a drastically lower threshold ratio of DOPE:DOPC = 1.5:1. Given that the PE content of eukaryotic membranes is significantly lower than that of most gram-negative bacterial membranes, the observed phase behavior of these AMO−membrane complexes suggests a mechanism for selectivity. This is in agreement with recent work highlighting the importance of lipid composition for AMP insertion.[35] [Note: We use conventional abbreviations for lipids. The first two letters indicate the length of the unsaturated hydrophobic alkyl chain (DO = 18 carbon atoms), and the second two letters indicate the structure of the hydrophilic head group: PE, phosphoethanolamine; PG, phosphoglycerol; PC, phosphocholine; PS, phosphoserine.]

Cellular membranes are more complex than lipid vesicles. Although a biological membrane cannot completely transform into a bulk inverted hexagonal phase, these results highlight structural tendencies of lipids when they interact with synthetic antimicrobials. We found good correlation between *in vitro* antibacterial activity and vesicle experiments for this system, and we expect the lipids in bacteria to exhibit similar tendencies in their interactions with these AMOs.

2. Experimental Section

2.1. AMO Preparation. The design principles leading to the development of mPE oligomers as AMP mimics have been reported.[25,30,36] These AMOs were prepared by Sonogashira chemistry, followed by deblocking of the nitrogen protecting groups; details are described elsewhere.[30,32] Typical purity of the AMOs, as found by HPLC, is 98%. Stock solutions of the AMOs in dimethylsulfoxide (DMSO):Millipore water 1:11 v:v were used for all experiments.

2.2. Vesicle Preparation for X-ray Experiments. All lipids were purchased from Avanti Polar Lipids and used without further purification. For X-ray experiments using purified lipids, we used sonication to prepare SUV vesicles of different compositions that mimic bacterial and mammalian membranes. Mixtures of DOPG (1,2-dioleoyl-*sn*-glycero-3-[phospho-*rac*-(1-glycerol)] (sodium salt)) and DOPE (1,2-dioleoyl-*sn*-glycero-3-phosphoethanolamine) were used as a first-order model for bacterial membranes. We used ternary mixtures of DOPG,

(17) Zasloff, M. *Proc. Natl. Acad. Sci. U.S.A.* **1987**, *84*, 5449−5453.
(18) Chen, Y.; Mant, C. T.; Farmer, S. W.; Hancock, R. E. W.; Vasil, M. L.; Hodges, R. S. *J. Biol. Chem.* **2005**, *280*, 12316−12329.
(19) Won, H.-S.; Jung, S.-J.; Kim, H. E.; Seo, M.-D.; Lee, B.-J. *J. Biol. Chem.* **2004**, *279*, 14784−14791.
(20) Hamuro, Y.; Schneider, J. P.; DeGrado, W. F. *J. Am. Chem. Soc.* **1999**, *121*, 12200−12201.
(21) Porter, E. A.; Wang, X.; Lee, H.-S.; Weisblum, B.; Gellman, S. H. *Nature* **2000**, *404*, 565−565.
(22) Liu, D.; DeGrado, W. F. *J. Am. Chem. Soc.* **2001**, *123*, 7553−7559.
(23) Epand, R. F.; Raguse, T. L.; Gellman, S. H.; Epand, R. M. *Biochemistry* **2004**, *43*, 9527−9535.
(24) Patch, J. A.; Barron, A. E. *J. Am. Chem. Soc.* **2003**, *125*, 12092−12093.
(25) Tew, G. N.; Liu, D.; Chen, B.; Doerksen, R. J.; Kaplan, J.; Carroll, P. J.; Klein, M. L.; DeGrado, W. F. *Proc. Natl. Acad. Sci. U.S.A.* **2002**, *99*, 5110−5114.
(26) Liu, D.; Choi, S.; Chen, B.; Doerksen, R. J.; Clements, D. J.; Winkler, J. D.; Klein, M. L.; DeGrado, W. F. *Angew. Chem., Int. Ed.* **2004**, *43*, 1158−1162.
(27) Tang, H.; Doerksen, R. J.; Tew, G. N. *Chem. Commun.* **2005**, 1537−1539.
(28) Kuroda, K.; DeGrado, W. F. *J. Am. Chem. Soc.* **2005**, *127*, 4128−4129.
(29) Ilker, M. F.; Nüsslein, K.; Tew, G. N.; Coughlin, E. B. *J. Am. Chem. Soc.* **2004**, *126*, 15870−15875.
(30) Arnt, L.; Tew, G. N. *J. Am. Chem. Soc.* **2002**, *124*, 7664−7665.
(31) Arnt, L.; Tew, G. N. *Langmuir* **2003**, *19*, 2404−2408.
(32) Arnt, L.; Nüsslein, K.; Tew, G. N. *J. Polym. Sci. A, Polym. Chem.* **2004**, *42*, 3860−3864.
(33) Ishitsuka, Y.; Arnt, L.; Majewski, J.; Frey, S.; Ratajczek, M.; Kjaer, K.; Tew, G. N.; Lee, K. Y. C. *J. Am. Chem. Soc.* **2006**, *128*, 13123−13129.
(34) Tew, G. N.; Clements, D.; Tang, H.; Arnt, L.; Scott, R. W. *Biochim. Biophys. Acta, Biomembr.* **2006**, *1758*, 1387−1392.

(35) Gidalevitz, D.; Ishitsuka, Y.; Muresan, A. S.; Konovalov, O.; Waring, A. J.; Lehrer, R. I.; Lee, K. Y. C. *Proc. Natl. Acad. Sci. U.S.A.* **2003**, *100*, 6302−6307.
(36) Arnt, L.; Rennie, J. R.; Linser, S.; Willumeit, R.; Tew, G. N. *J. Phys. Chem. B* **2006**, *110*, 3527−3532.

DOPE, and DOPC (1,2-dioleoyl-*sn*-glycero-3-phosphocholine) as a more realistic model for the heterogeneous distribution of lipids in real bacterial membranes. These ternary membranes also allowed us to vary the intrinsic membrane curvature independently from the membrane charge density. Mixtures of DOPS (1,2-dioleoyl-*sn*-glycero-3-[phospho-L-serine] (sodium salt)) and DOPC were used as models for animal membranes. DOPG or DOPS stock solutions in chloroform/methanol solution were mixed with DOPC and/or DOPE stock solutions in chloroform solution; all stock solutions were at 30 mg/mL. The mixture was dried under N_2, desiccated under vacuum, hydrated with Millipore water to a final lipid concentration of 25 mg/mL, and incubated overnight at 37 °C. The resultant solution was sonicated to clarity and extruded through a 0.2-μm Nucleopore filter to get SUVs. All experiments were carried out at room temperature, which is much higher than the gel−liquid phase transition temperature for any of the component lipids (T_m (°C): DOPG, −18; DOPE, −16; DOPC, −20), so there is no phase separation in the SUV membranes.

For X-ray experiments using vesicles composed of *Escherichia coli* lipid extracts, we prepared unilamellar vesicles using extrusion, since sonication produces vesicles larger than 200 nm when *E. coli* extract is used. *E. coli* lipid extracts in chloroform/methanol stock solutions were dried under N_2, desiccated in vacuum overnight, and hydrated with Millipore water at 45 °C for 2 h. The resultant solution was subjected to five freeze−thaw cycles and subsequently extruded through 0.2-μm Nucleopore membranes 11 times.

2.3. X-ray Diffraction. AMO solutions were mixed with vesicle solutions and sealed in quartz capillaries for SAXS experiments. For in-house SAXS experiments, incident Cu Kα radiation ($\lambda = 1.54$ Å) from a Rigaku rotating-anode generator was monochromatized and focused using Osmic confocal multilayer optics and collimated to a final beam size of ~0.8 × 0.8 mm². Scattered radiation was collected on a Bruker 2D multiwire detector (pixel size, 105 μm). For SAXS experiments at the Stanford Synchrotron Radiation Laboratory (BL4-2) and at the Advanced Photon Source (BESSRC-CAT BL-12IDC), monochromatic X-rays with energies of 9 and 12 keV, respectively, were used. The scattered radiation was collected using a MAR Research CCD area detector (pixel size, 79 μm). No radiation damage was observed for the exposure times used. Electron density profiles of unit cells were calculated using Fourier synthesis techniques for centrosymmetric systems.[37−40]

2.4. Antibacterial Activity Assays. This procedure is a modification of the standard broth microdilution assay recommended by the NCCLS.[6,34] Bacteria were grown in Mueller−Hinton broth at 37 °C overnight, and the bacterial growth was measured by optical density at $\lambda = 600$ (OD_{600}) using an Eppendorf BioPhotometer. After the regrowth of bacteria ($OD_{600} = 0.5-0.6$), the suspension was diluted to ~5 × 10⁵ CFU/mL and inoculated into a polypropylene (Costar) 96-well round-bottom plate (90 μL volumes). A solution containing DMSO without the compound was prepared as a negative control. Compound stock solutions were prepared in DMSO, and serial two-fold dilutions of compound were made in 0.01% acetic acid and 0.2% bovine serum albumin directly in the wells of the polypropylene plate at 10 μL/well. DMSO concentrations did not exceed 1% in the assay. One set of control wells included broth-only samples with dilution buffer for testing sterility and providing blank values for the assay readings. Vehicle-control wells containing the bacterial suspension with DMSO (no compound) were also included. The assay plate was incubated at 37 °C for 18 h. The MIC was measured by observing the presence of cell growth, defined by the NCCLS as a ≥2 mm button or definite turbidity.

2.5. Hemolytic Activity Assays. Compound stock and control solutions were prepared by the same procedure in the antimicrobial activity assay. Fresh human red blood cells (RBCs) were obtained by centrifuging whole blood (3000 rpm, 10 min) to remove plasma and white blood cells. The RBCs (1 mL) were diluted with 9 mL of TBS buffer (10 mM Tris buffer, pH 7.0, 150 mM NaCl), and this suspension was further diluted by a factor of 40 to give a RBC stock suspension (0.25% blood cells). This RBC stock (120 μL), TBS buffer (15 μL), and the compound stock solutions (15 μL) (or control solutions) were added to a 200-μL centrifugation tube and incubated at 37 °C for 1 h. The tube was centrifuged at 4000 rpm for 5 min. Supernatant (30 μL) was diluted with TBS buffer (100 μL), and the OD_{414} of the solution was measured as a function of hemoglobin concentration. Melittin was used as a positive control, and the most concentrated sample (100 μg/mL) was used as a reference for 100% hemolysis. A control solution containing only DMSO was used as a reference for 0% hemolysis.

2.6. Lipid-Composition-Dependent Vesicle Leakage Assay Using Calcein. Vesicles of different lipid compositions were prepared with extrusion as described above. The following buffers were used in the calcein leakage experiments: buffer A, 40 mM calcein, 10 mM Na_2-HPO_4, pH 7.0; buffer B, 10 mM Na_2HPO_4, 90 mM NaCl, pH 7.0. Specifically, *E. coli* lipid extract and egg yolk PC (EYPC) were mixed in chloroform solution at 25 mg/mL to a total volume of 500 μL. These mixtures were evaporated at reduced pressure on a rotary evaporator and then in vacuum overnight. The resulting film was hydrated for 1 h with 1 mL of buffer A. The resulting suspension was subjected to five freeze−thaw cycles and subsequently extruded through a 0.4-μm Whatman polycarbonate membrane >10 times. The external calcein was removed by gel filtration (Sephadex G-50) using buffer B, and the resulting 1.0 mL of vesicle solution was diluted further with buffer B to 6 mL; 20 μL of this solution was added to 1.98 mL of buffer B in a fluorescence cuvette. Fluorescence emission intensity I_t ($\lambda_{em} = 510$ nm, $\lambda_{ex} = 450$ nm) was monitored as a function of time (t) during addition of AMO-1, AMO-2, AMO-3, and 20% Triton X-100 in DMSO. Flux curves are normalized to percentage leakage [$(I_t − I_0)/(I_\infty − I_0)] \times 100$. I_0 is I_t before the addition of AMO-1, AMO-2, or AMO-3, and I_∞ is I_t after addition of Triton-X.

2.7. Size-Dependent Vesicle Leakage Assay Using Encapsulated Fluorescent Macromolecules of Different Molecular Weights. GUVs were prepared using the swelling method. *E. coli* lipid extract in chloroform was deposited (100 μL at 20 mg/mL) onto roughened, cleaned Teflon, dried under vacuum, and then hydrated with 5 mL of 100 mM sucrose solution (for inverted confocal microscopy) or 100 mM glucose solution (for upright fluorescence and polarized microscopy) and incubated for 2−3 days at 37 °C.[41,42] For upright fluorescence microscopy, the membrane dye β-BODIPY FL C_5-HPC (Invitrogen) was mixed with the lipids in chloroform to a total concentration of 1 mol %. For size-dependent dye leakage experiments, C_5 maleimide (1 kDa) labeled with the fluorophore Alexa Fluor 546, and dextran (10 kDa) labeled with Alexa Fluor 488 (both, Invitrogen), were incorporated into the sucrose swelling solution at concentrations of 20 μM each. After swelling, GUV suspensions were diluted by 40× into 200 mM glucose (for inverted viewing) or 200 mM sucrose (for upright viewing). For viewing under crossed polarizers, AMO-2 in DMSO solution was added to the vesicle suspension at a concentration of 1:2 AMO-2:lipid and mixed by pipetting. For confocal viewing of size-dependent dye release, AMO-2 in DMSO solution was added to the vesicle suspension by dialysis across a membrane (Fisher) so that the same GUVs could be viewed continuously; concentrations of 0.1:1 to 1:1 AMO-2:lipid were used. We used a Leica SP2 laser scanning confocal microscope to observe GUVs. Laser lines of 488 and 543 nm were used for dye excitation at approximately 20% of their maximum intensity. A 60× water immersion lens was used to image the vesicles, with an aperture setting of one Airy unit at 488 nm. Each of the two exciting laser

(37) Harper, P. E.; Mannock, D. A.; Lewis, R. N. A. H.; McElhaney, R. N.; Gruner, S. M. *Biophys. J.* **2001**, *81*, 2693−2706.
(38) Turner, D. C.; Gruner, S. M. *Biochemistry* **1992**, *31*, 1340−1355.
(39) Francescangeli, O.; Pisani, M.; Stanic, V.; Bruni, P.; Weiss, T. M. *Europhys. Lett.* **2004**, *67*, 669−675.
(40) Henry, N. F. M.; Lonsdale, K. *International Tables for X-ray Crystallography*, 3rd ed.; The Kynoch Press: Birmingham, 1969; Vol. I, p 372.

(41) Needham, D.; Evans, E. *Biochemistry* **1988**, *27*, 8261−8269.
(42) Tamba, Y.; Yamazaki, M. *Biochemistry* **2005**, *44*, 15823−15833.
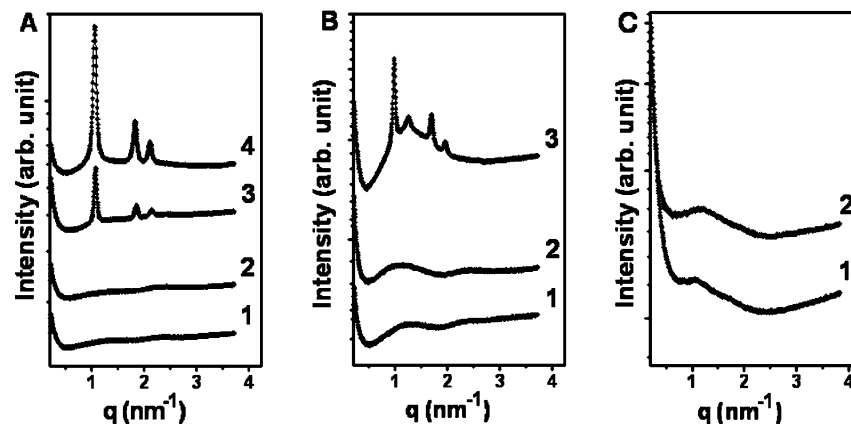
Figure 1. (A) For DOPG:DOPE = 20:80 membranes, the SAXS data for the inactive AMO-1 are essentially the same as those for vesicles alone (curves 2 and 1). For both the specifically active AMO-2 (curve 3) and nonspecifically active AMO-3 (curve 4), an inverted hexagonal phase is induced. (All AMO concentrations are 158 μg/mL.) (B) In complexes formed between the specifically active AMO-2 and *E. coli* lipid extracts, the same trends are observed: the inverted hexagonal phase is not present for complexes with AMO-1 and for the lipid extract alone (curves 2 and 1) but is clearly visible for complexes with AMO-2 (curve 3). Phase separation, indicated by an additional peak (see text), is also observed. This is consistent with the more complex lipid distribution expected from bacterial membrane extracts. (C) For DOPS:DOPC = 20:80 membranes, no peaks from the inverted hexagonal phase are observed for lipid vesicles alone (curve 1) or for the same vesicles mixed with specifically active AMO-2 (curve 2), despite the fact that these vesicles have the same charge density as the bacterial membrane mimics used in (A).

frequencies and fluorophore emissions was independently scanned sequentially, line-by-line, to produce 512 × 512 pixel images in 2−3 s.

3. Results and Discussion

3.1. Antibacterial Activity of AMOs. We test AMO activity against *E. coli* and *B. subtilis* since these species are reliable markers for broad Gram-negative and Gram-positive antibacterial activity[25,34,43] and against human RBCs as representative mammalian cells. AMO-2 exhibits excellent antibacterial activity against *E. coli* and *B. subtilis* (as shown in Table 1) and against a wide range of bacteria including MRSA and VRE, against which it has a minimal inhibition concentration (MIC) of 0.5 μg/mL.[34] The concentration required to cause 50% hemolysis (HC$_{50}$) shows that AMO-2 is >44 times more cytotoxic against bacteria than RBCs. Our results are in agreement with previous work showing that AMO-2 is potently antimicrobial yet nontoxic to human RBCs.[26,27,34,43] When the ethylamine group of the specifically active AMO-2 is shortened to a single methylene (AMO-1), all activity against both bacteria and RBCs is lost. In contrast, when the ethylamine group is extended to propylamine (AMO-3), the AMO shows activity against both bacteria and RBCs. These structurally similar AMOs span the whole range of activity profiles: completely inactive (AMO-1), specifically active (AMO-2), and nonspecifically active (AMO-3). We use this series of oligomers to investigate the relationship among activity, specificity, and structural reorganization at different membrane compositions.

3.2. Correlation between Antibacterial Activity and AMO− Membrane Self-Assembly: Active AMOs Cooperatively Transform SUVs of Model Bacterial Membranes to an Inverted Hexagonal Phase. In this experiment, DOPG:DOPE = 20:80 vesicles are used to mimic gram-negative bacterial membranes. For complexes formed between DOPG:DOPE vesicles and AMO-1, the SAXS data are essentially the same as those for the DOPG:DOPE vesicles alone (Figure 1A, curves 1 and 2): only weak broad form factor features are visible,

suggestive of intact unilamellar vesicles with no significant AMO-induced membrane remodeling.

For complexes formed with the specifically active AMO-2, three peaks were observed at 1.085, 1.880, and 2.176 nm^{-1} (Figure 1A, curve 3). The q positions of these three peaks have the relative ratios of $1:\sqrt{3}:2$, which is characteristic of a hexagonal structure. The unit cell parameter of this hexagonal structure is $a = 4\pi/(q_{10}\sqrt{3}) = 6.69$ nm. Complexes formed with the nonspecifically active AMO-3 exhibit three peaks at the same characteristic ratio and can be indexed to a hexagonal structure with a slightly larger unit cell parameter, $a = 6.86$ nm (Figure 1A, curve 4). [Note: AMO-1, AMO-2, and AMO-3 are all divalent cations that can bind to anionic membranes. The size differences between them are not large and do not traverse any fundamental length scales, such as the Gouy− Chapman length or the Bjerrum length, so we do not expect drastic changes in their membrane binding behavior.]

The same trends are observed for AMO−membrane complexes formed using *E. coli* lipid extract (Figure 1B). Curves 1 and 2 in Figure 1B show that SAXS data from complexes formed using the inactive AMO-1 are similar to those obtained from only the *E. coli* lipid extract vesicles without any AMO present. Moreover, curve 3 in Figure 1B shows that AMO-2 induces a hexagonal structure ($a = 7.38$ nm) similar to that induced in DOPG:DOPE = 20:80 model membranes. In addition, a peak is observed at $q = 1.256$ nm^{-1}, which corresponds roughly to a periodicity equal to the thickness of the membrane plus that of the AMO. These results suggest that hexagonal and lamellar structures coexist; we attribute this to phase separation in the more complex distribution of lipids in bacterial extracts.

In contrast to its activity against model bacterial membranes, the specifically active AMO-2 does not restructure membranes composed of DOPS:DOPC, a composition that mimics that of mammalian membranes. Typical SAXS data from DOPS:DOPC = 20:80 AMO−membrane complexes are essentially identical to those from vesicle solutions without added AMO (Figure 1C).

In order to elucidate the structure of the observed hexagonal phase, we performed electron density $\rho(x,y)$ reconstructions of

(43) Tang, H.; Doerksen, R. J.; Jones, T. V.; Klein, M. L.; Tew, G. N. *Chem. Biol.* **2006**, *13*, 427−435
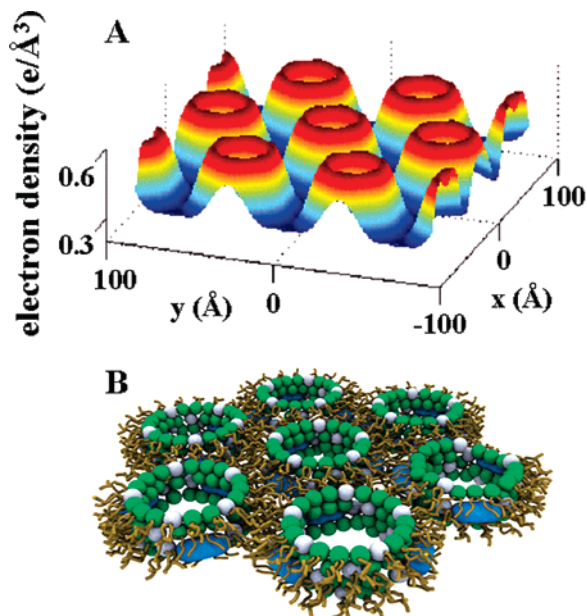
Figure 2. (A) Electron density profile $\rho(x,y)$ of the 2D unit cell for complexes formed by the specifically active AMO-2 and DOPG:DOPE = 20:80 lipid membranes, confirming the inverted hexagonal structure. The regions of lowest electron density correspond to lipid chains. Circular "rims" of high electron density surrounding "holes" of intermediate density correspond to lipid head groups surrounding water channels which have a diameter of ~3.4 nm. (B) A proposed model of the unit cell. The white and green spheres represent head groups of zero intrinsic curvature (ex. DOPG, DOPC) and negative intrinsic curvature lipids (ex. DOPE), respectively. AMO-2 molecules are represented by blue spherocylinders embedded in the membrane.

the 2D hexagonal unit cell, where x and y are mutually perpendicular axes. Figure 2A shows the $\rho(x,y)$ profiles of the self-assembled complex between AMO-2 and DOPG:DOPE = 20:80 membranes. Only one choice of the phases $(+,-,-)$ for the amplitudes at q_{10}, q_{11}, and q_{20} corresponds to membrane structures with physically realizable sizes and spatial distributions of hydrophilic and hydrophobic parts. This choice of phase results in electron densities consistent with an inverted hexagonal phase (H_{II}) and is also consistent with the phase of previous reconstructions of lipid-only H_{II} phases.[38] Lipids typically have a high average electron density near the head groups (~0.46 e/Å^3) and a low density in the hydrocarbon tails (~0.30 e/Å^3), while water has an intermediate density of 0.33 e/Å^3. The lowest density regions in Figure 2A correspond to hydrocarbon chains of the lipids, while the circular "rims" of high electron density surround "holes" of intermediate density that correspond to the phospholipid head groups surrounding water channels. The effective diameter of the water channel in the H_{II} phase is measured to be ~3.4 nm. We obtain a similar electron density reconstruction for AMO-3. Formation of the H_{II} phase is consistent with the expectation that a high volume fraction of negative-curvature lipids (such as DOPE) will favor an inverted hexagonal phase rather than a hexagonal phase (see Note at the end of this paragraph). Interestingly, the behavior of AMPs is significantly different from that of the AMOs, which are too small to span the thickness of a typical membrane. For example, magainin has been observed to induce positive rather than negative membrane curvature,[12,45] which is consistent with our
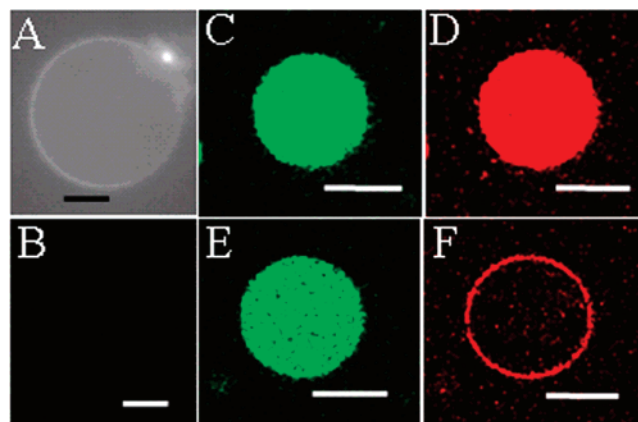
(44) Lewis, R. N. A. H.; McElhaney, R. N.; Harper, P. E.; Turner, D. C.; Gruner, S. M. *Biophys. J.* **1994**, *66*, 1088−1103.

Figure 3. A representative GUV viewed using (A) fluorescence microscopy and (B) transmitted light under crossed polarizers. (C−F) Representative two-channel (false-colored green and red) size-dependent leakage from a single GUV using confocal fluorescence microscopy before (C,D) and after (E,F) treatment with AMO-2. Small molecules (D) (molecular weight 1 kDa, red) are released (F), but large molecules (C) (molecular weights averaging 10 kDa, green) are mostly retained (E). Scale bars = 10 μm.

SAXS results for pexigainin, a magainin derivative. [Note: The electron density of the circular "rim" is about ~0.56 e/Å^3, which is higher than typical values for phospholipid head groups. This suggests that the AMO, which contains high-electron-density bromines, stays close to the membrane surface, in agreement with recent experiments on AMO-2 insertion into lipid mono-layers at the air−water interface.[33] This localization to the amphiphilic interface should impact strongly on the lipid phase behavior: lipids with additional steric volume near the interface have a drastically increased propensity to form inverted phases.[44]]

We investigated the cooperativity of the AMO-induced reconstruction by varying the concentration of AMOs. SAXS data show that the inverted hexagonal H_{II} phase (DOPG:DOPE = 20:80) can be induced by the specifically active AMO-2 and nonspecifically active AMO-3 at different AMO concentrations starting from 40 μg/mL, which correspond to AMO:lipid molar ratios of 1:84 to 1:21 and are well below that at the MIC (~300:1, with variations depending on approximations used) for *E. coli*. [Note: In a growth inhibition assay, there are ~10^5 cells in 1 mL of medium, and the approximate number of lipids per cell is ~2.2 × 10^7, leading to a total lipid concentration of ~3.65 × 10^{-3} μM. The MIC of AMO-2 is 1.3 μM. This translates to an AMO:lipid molar ratio of 300:1 at this AMO-2 concentration. In the SAXS experiments, 40 μg/mL of AMO-2 induced an H_{II} phase in model membranes at 4 mg/mL lipid concentration. The AMO-2:lipid molar ratio for the SAXS experiments is 1:80 at this AMO concentration.]

3.3. Specifically Active AMO Induces Molecular-Weight-Dependent Leakage of Quasi-2D Membranes in GUVs. We may expect that the AMO-induced structural tendency to enforce negative curvature and form an H_{II} phase is expressed differently in a quasi-2D membrane geometry that is more representative of a bacterial membrane. To investigate this, we treat GUVs with AMO-2 and view them under a microscope.[46] A fluorescent membrane dye allows us to locate the vesicle, which remains

(45) Huang, H. W. *Biochim. Biophys. Acta, Biomembr.* **2006**, *1758*, 1292−1302.

(46) Dong, W.-F.; Liu, S.; Wan, L.; Mao, G.; Kurth, D. G.; Möhwald, H. *Chem. Mater.* **2005**, *17*, 4992−4999.
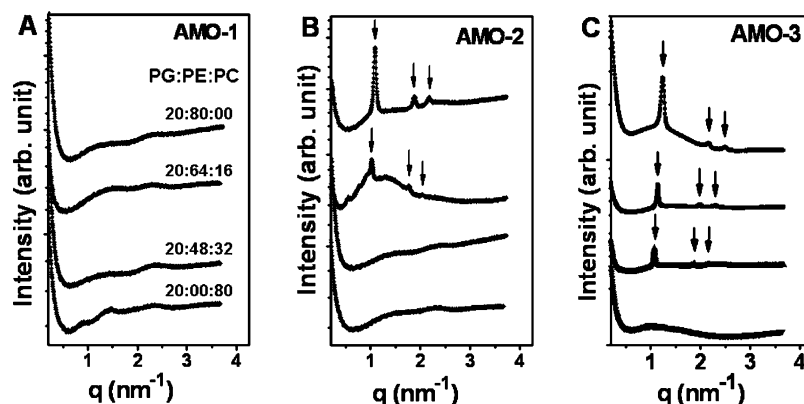
Figure 4. Antimicrobials with different activity profiles require different concentrations of DOPE in the target membrane to induce the inverted hexagonal phase. In each panel, from top to bottom, we show SAXS data for the structures formed by an AMO complexed with membranes of decreasing DOPE compositions (DOPG:DOPE:DOPC = 20:80:00, 20:64:16, 20:48:32, and 20:00:80). Arrows indicate the peak positions of the inverted hexagonal phase. For the inactive AMO-1 (A), the inverted hexagonal phase is never observed, even for the highest DOPE content. For the specifically active AMO-2 (B), the inverted hexagonal phase is formed only when the DOPE content is above a minimum threshold concentration of 64%. (C) The nonspecifically active AMO-3 is able to induce the inverted hexagonal structure at the lowest DOPE content (48%) and does so at an AMO concentration that is about one-fourth that in (B) and (A), which are fixed at 158 μg/mL. Since the PE content of eukaryotic cell membranes is significantly lower than that of gram-negative bacterial membranes, this suggests that negative-curvature lipids may contribute to the mechanism of antimicrobial specificity.

spherical and appears unchanged after treatment with AMO-2 (Figure 3A). Since the H_{II} phase is a dense 3D phase with a different topology than that of a quasi-2D GUV membrane, this indicates that the bulk H_{II} phase is not formed here. In agreement with this inference, when viewed under crossed-polarizers using transmitted light, the vesicle appears dark (Figure 3B), without observable birefringence, which would be expected from the H_{II} phase. To check what structure is induced by active AMOs on the membranes of intact GUVs, we load vesicles with dyed molecules of two different sizes, 10 kDa ($\sim$5.4 nm, Figure 3C) and 1 kDa ($\leq$2 nm, Figure 3D).[46−49] When AMO-2 is applied to these vesicles, the small molecules are released (Figure 3F) and the large molecules are retained (Figure 3E), suggesting that holes of a size bigger than the small molecule but smaller than the large molecule likely formed in the GUV (see Note at the end of this paragraph). These results provide valuable guidance on understanding how the AMO-induced structural tendency toward the H_{II} phase may be expressed in 2D systems. [Note: The membrane of the AMO-treated GUV exhibits a bright fluorescence signal from the dye tagged to the maleimide (red outline in Figure 3F). We hypothesize that this is caused by the electrostatic attraction between the negatively charged maleimide molecule and the positively charged amine groups on AMO-2 molecules inserted into the membrane. It is notable that maleimide shows no preferential association with membranes that have not been treated with AMO.]

In our confocal experiments, we observe leakage from intact vesicles, which shows that pores have been formed. The topological requirement for pore formation is negative Gaussian membrane curvature.[50] This is the type of "saddle-shaped" curvature on the insides of donut holes, which have positive curvature along one principal direction and negative curvature along the other at a given point on a 2D surface. In the SAXS experiments, we see the induction of an H_{II} phase, which requires the generation of negative curvature, which is a

necessary (though not sufficient) condition for generating negative Gaussian curvature. We hypothesize that negative-curvature lipids are recruited by this family of antimicrobials to form the negative curvature along the pore circumference in the plane of the membrane. Pores also have positive curvature along the orthogonal direction. Our present experiments are not sensitive to the physical origin of this positive curvature. Such curvature may be generated in different ways, for example, by local enrichment in positive-curvature lipids or by antimicrobial-induced reorientation of alkyl chains in negative- or zero-curvature lipids.

3.4. Specificity of AMO Activity Is Observed in Sensitivity of Induced Membrane Reconstruction to Changes in DOPE Concentration. The specifically active AMO-2 induces an inverted hexagonal phase H_{II} in PG:PE membranes that mimic gram-negative bacterial membrane compositions but does not induce this phase for PS:PC membranes that mimic eukaryotic membrane compositions. To understand this, we isolate membrane charge from intrinsic membrane curvature using ternary lipid membranes with constant charge and tunable intrinsic curvature, C_0. Specifically, we change the ratio of DOPE ($C_0 < 0$) to DOPC ($C_0 \approx 0$) at a fixed DOPG concentration (20%) and determine the structures formed when this model interacts with our three AMOs.

The SAXS data in Figure 4 show how the inactive, specifically active, and nonspecifically active forms of AMOs interact and self-assemble with membranes at four different lipid compositions (DOPG:DOPE:DOPC ratios of 20:80:00, 20:64:16, 20:48:32, and 20:00:80). For AMO-1 (Figure 4A), there is no significant restructuring of the membrane vesicles across the entire range of DOPE concentration examined up to DOPG:DOPE = 20:80, and the H_{II} phase is never observed. For the specifically active AMO-2 (Figure 4B), the H_{II} phase is observed only when the DOPE content is above a minimum threshold concentration of 64% (unit cell parameter $a = 6.71$ and 7.11 nm for membranes with DOPG:DOPE:DOPC = 20:80:00 and 20:64:16, respectively). As the concentration of DOPE drops below 64%, the peaks for the H_{II} phase disappear, indicating that this specifically active AMO cannot generate the H_{II} phase

(47) Lebrun, L.; Junter, G.-A. *J. Membr. Sci.* **1994**, *88*, 253−261.
(48) Hanselmann, R.; Burchard, W.; Lemmes, R.; Schwengers, D. *Macromol. Chem. Phys.* **1995**, *196*, 2259−2275.
(49) Mwangi, J. W.; Ofner, C. M., III. *Int. J. Pharm.* **2004**, *278*, 319−327.
(50) Gelbart, W. M.; Ben-Shaul, A.; Roux, D. *Micelles, Membranes, Micro-emulsions and Monolayers*, 1st ed.; Springer: New York, 1994.
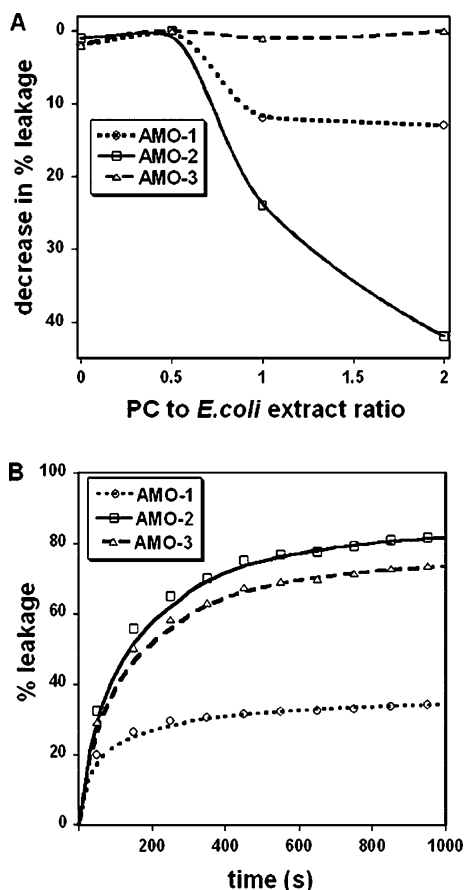
Figure 5. (A) Fluorimetry quantifies the AMO-induced dye leakage from *E. coli* lipid extract vesicles with increasing concentration of EYPC. The decrease in percent leakage of calcein from the vesicles is plotted versus the ratio of EYPC to *E. coli* lipid extract (0:1, 0.5:1, 1.5:1, 2:1) upon addition of AMO-1 (dotted line), AMO-2 (solid line), and AMO-3 (dashed line). The leakage decreases significantly for AMO-2 as the concentration of PC increases or as the concentration of natural PE lipid decreases. In addition, AMO-3 is insensitive to the concentration of PC, showing no decrease leakage over the entire range of PE volume fraction studied. AMO-1 shows a slight dependence on PC concentration, but, as shown in (B), this molecule causes significantly less leakage than AMO-2 or AMO-3.

at reduced DOPE concentrations. In contrast, the nonspecifically active AMO-3 is able to induce the H$_{II}$ phase even down to a DOPE concentration of 48%, unlike AMO-2 (Figure 4C). We carried out similar SAXS experiments using model lipid membranes composed of DOPS:DOPE:DOPC to mimic eukaryotic membranes, and the same trends were observed. (These effects are, in fact, even more accentuated in DOPS-based membranes, with a lower threshold fraction of DOPE for AMO-3.) The differences in concentrations of negative-curvature lipids

in bacterial and eukaryotic membranes may provide a mechanism for the AMO specificity observed for AMO-2, as indicated by the fact that the PE:PC ratio of the target membrane directly influences the ability of these AMOs to induce the inverted hexagonal phase in bulk.

In an analogous experiment on quasi-2D membranes, we use fluorimetry to quantify the amount of dye leakage from vesicles with compositions that mimic bacterial and eukaryotic membranes. When vesicles containing the tracer dye calcein are treated with AMO-2, we measure more leakage from PG:PE 10:90 vesicles than from PS:PC 10:90 vesicles.[36] This is consistent with our hypothesis that membrane composition is part of the mechanism for antibacterial selectivity. We also test membrane vesicles composed of *E. coli* lipid extract diluted with increasing concentrations of zero-curvature PC lipid to alter the PE:PC ratio. Figure 5A shows the decrease in leakage for each AMO as the concentration of PE lipid is reduced by PC. AMO-2 shows the largest dependence on PE volume fraction, with a decrease in leakage from 80% for pure *E. coli* extract vesicles to 39% for 1:2 *E. coli* extract:PC vesicles. In contrast, AMO-3 shows approximately 72% leakage for all vesicle compositions, indicating that AMO-3 has no dependence on the PE volume fractions studied here. AMO-1 shows a ~10% decrease in leakage and exhibits significantly less overall dye leakage than AMO-2 or AMO-3 (Figure 5B). These observations are all consistent with our assays of the biological activity of these AMOs and with our hypothesis of intrinsic membrane curvature as a mechanism for antimicrobial specificity.

4. Conclusions

We investigated how a prototypical family of synthetic AMOs remodels membrane vesicles of different compositions using synchrotron SAXS and confocal microscopy. Antibacterial activity is correlated with an AMO-induced structural tendency to induce negative curvature in membranes. Moreover, the ability of these AMOs to restructure membranes is critically dependent on the concentration of negative-curvature lipids in a given membrane, which suggests that such lipids may play a critical role in the selective action of antimicrobials.